

Two-qubit parametric amplifier: large amplification of weak signals

S. Savel'ev^{1,2}, A.M. Zagoskin^{1,2}, A.L. Rakhmanov^{3,2,1}, A.N. Omelyanchouk^{2,4}, Z. Washington¹, Franco Nori^{2,5}

¹*Department of Physics, Loughborough University, Leicestershire, LE11 3TU, United Kingdom*

²*Advanced Science Institute, RIKEN, Wako-shi, Saitama 351-0198, Japan*

³*Institute for Theoretical and Applied Electrodynamics,
Russian Academy of Sciences, 125412 Moscow, Russia*

⁴*B.Verkin Institute for Low Temperature Physics and Engineering, 61103, Kharkov, Ukraine*

⁵*Physics Department, The University of Michigan, Ann Arbor, MI 48109-1040, USA*

Using numerical simulations, we show that two coupled qubits can amplify a weak signal about hundredfold. This can be achieved if the two qubits are biased simultaneously by this weak signal and a strong pump signal, both of which having frequencies close to the inter-level transitions in the system. The weak signal strongly affects the spectrum generated by the strong pumping drive by producing and controlling mixed harmonics with amplitudes of the order of the main harmonic of the strong drive. We show that the amplification is robust with respect to noise, with an intensity of the order of the weak signal. When deviating from the optimal regime (corresponding to strong qubit coupling and a weak-signal frequency equal to the inter-level transition frequency) the proposed amplifier becomes less efficient, but it can still considerably enhance a weak signal (by several tens). We therefore propose to use coupled qubits as a combined parametric amplifier and frequency shifter.

I. INTRODUCTION

While the desire of building code-cracking quantum computers [1] remains as elusive as ever since its inception, its pursuit has been one of the major contributing factors to the enormous progress achieved in quantum mesoscopic physics and quantum nanodevices over the last decade and a half. These efforts have already resulted in the development of a new branch of mesoscopic digital and analogue devices [2–7] and even new types of materials known as quantum metamaterials [8, 9], allowing to control quantum coherent media. In this article we describe how two coupled qubits can be used as a parametric amplifier.

A. Superconducting qubits

From the point of view of quantum computing, a qubit is any two-state quantum system which satisfies certain control and readout requirements and can therefore be used for the execution of quantum algorithms (see, e.g., [1], Ch. 2). Many efforts have been devoted to the study of theoretical quantum information processing and, more recently, significant progress has been achieved on experimental aspects of this field. For example, one of the most fascinating results obtained in experimental mesoscopic physics over the past decade has been the realization of several types of superconducting qubits, which demonstrated many of the qualities required for quantum information processing. Moreover, superconducting qubits in quantum electronics have a potentially much wider range of applications than just quantum information processing (see, e.g., Refs. [2–4, 8, 10–12]), including: single-photon generators, producing quantum (squeezed or Fock) states of the electromagnetic field, quantum transmission lines, quantum amplifiers, etc. Various types of superconducting qubits have been produced, including charge, flux, and phase qubits. These use different physical mechanisms to control their states and store information. For example, in a charge qubit, the state $|1\rangle$ has one extra Cooper pair, compared to the state $|0\rangle$, while for a flux qubit, the two logical states differ by a fraction of the magnetic flux quantum. Superconducting qubits are mesoscopic (e.g., their working quantum states may differ by dozens of millions of single-particle states) and scalable (i.e., it is possible to link these together). Moreover, their fabrication, control, and readout require techniques already well developed in solid state electronics.

Several superconducting qubit designs of various degrees of complexity and performance have been realized (reviewed in, e.g., Refs. 2, 3, 5, 10–12). The so-called persistent-current flux qubit [13, 14] combines relative simplicity with decent decoherence times and scalability. It consists of a small superconducting loop (approximately $10\ \mu\text{m}$ across) interrupted by three Josephson junctions. The flux quantization condition is

$$\phi_1 + \phi_2 + \phi_3 + 2\pi\Phi/\Phi_0 = 2\pi n, \quad (1)$$

where ϕ_j is the phase difference across the j th junction, Φ is the total magnetic flux through the loop, $\Phi_0 = h/2e$, and n is an integer. This allows to eliminate one of the phases (e.g., ϕ_3). Due to the small self-inductance of the loop, the difference between the flux Φ and the external flux Φ_x , as well as the magnetic energy of the system, can be neglected. On the other hand, one must include the contribution to the energy from the charges on the Josephson

junctions, $Q_j^2/2C_j$, and the Josephson energy $-E_j \cos \phi_j$, where C_j and E_j is the capacitance and the Josephson energy of the j th junction, respectively. Up to numerical factors, the junction charges are the momenta canonically conjugate to the Josephson phase differences (see, e.g., [15], §2.3). Introducing variables $\phi_{\pm} = (\phi_1 \pm \phi_2)/2$, it is straightforward to show that the classical Hamilton function of the system (assuming that two junctions are identical, $C_1 = C_2 = C, E_1 = E_2 = E$, and that $C_3 = \alpha C, E_3 = \alpha E$) is given by

$$\mathcal{H} = \frac{\Pi_+^2}{2M_+} + \frac{\Pi_-^2}{2M_-} - E \left[2 \cos \phi_+ \cos \phi_- + \alpha \cos \left(2\phi_- + 2\pi \frac{\Phi_x}{\Phi_0} \right) \right], \quad (2)$$

where Π_{\pm} are the corresponding momenta and M_{\pm} are determined by the junction capacitances. The potential energy term in the interval is periodic and, for the proper choice of α and with $\Phi_x \approx \Phi_0/2$, it contains a double well, the minima of which are almost degenerate and correspond to the current flowing (counter)clockwise around the loop. These states are chosen as physical qubit states. Transitions between them are enabled by quantum tunneling through the barrier. The quantum-mechanical Hamiltonian of the persistent-current qubit is obtained from (2) by using the relation $\hat{N} = -i\partial/\partial\phi$ between the superconducting phase and the number of extra Cooper pairs (proportional to the charge on the Josephson junction). Its detailed analysis is given in [13, 14]. Truncating the Hilbert space of the system to the two lowest states, which can be done due to the strong anharmonicity of the potential in (2), its Hamiltonian can be reduced to the standard pseudospin form,

$$H = -\frac{1}{2}(\epsilon \sigma_z + \Delta \sigma_x). \quad (3)$$

Here ϵ is proportional to the external flux through the qubit, and Δ is determined by the tunneling matrix element between the potential minima. Here we note that persistent-current flux qubits have decoherence times in excess of $10 \mu\text{s}$ at the operating frequency $\sim 1 \text{ GHz}$, allow successful coherent coupling of several qubits, and show steady improvements. Therefore, these superconducting qubits are promising new elements for versatile quantum circuits.

B. Parametric amplifiers

A parametric amplifier is based on the idea of a parametric resonance occurring for a linear oscillator with parameters oscillating in time. Such an amplifier [16] is implemented as a mixer, where an input weak signal is mixed with a strong local oscillator signal producing the strong output.

In recent years, several new mesoscopic systems have been proposed and implemented as parametric amplifiers. These systems include small molecules in intense laser fields [17], polaritons in semiconductor microcavities [18], current-voltage oscillations in SQUIDs [19] and Josephson junctions [20–22]. Another proposal uses active and tuneable metamaterials [23] to amplify weak signals. Most of these proposals wish to develop a very compact parametric amplifier, which can even demonstrate quantum amplification [24]. This indicates that quantum qubit systems (and, in particular, superconducting qubit systems) could be very promising candidates for mesoscopic parametric amplifiers.

C. Outline of results

The main results of this work can be summarized as follows.

- Consider an ac drive $A \sin(\omega t)$ applied to a four-level quantum system (e.g., a couple of flux qubits (e.g., 26, 27) placed in an ac magnetic field, see Fig. 1) with $\omega_{\text{pump}} = \omega$ in resonance with a transition between a pair of its energy levels. Even though the evolution of the density matrix is described by a linear equation, the spectrum of the density matrix elements (Fig. 2) shows a sequence of peaks corresponding to different harmonics of the ac drive (which is commonly thought to occur only in nonlinear systems). More interestingly, the strongest oscillations are not at the main frequency ω , but at some of its harmonics, forming a hierarchy of resonances, which is unusual for nonlinear systems. The explanation of this phenomenon lies in the structure of the master equations' set for the density matrix elements, in which the external signal enters multiplicatively rather than additively.
- Such a *hierarchy of parametric resonances* makes this two qubit system (e.g., two coupled flux qubit) an efficient parametric amplifier and frequency shifter, especially if the weak signal has its frequency $\omega_{\text{weak}} = \tilde{\omega}$ close to another inter-level transition of the system. The latter can be achieved by tuning the qubit coupling (e.g., like in Ref. 27, see also Fig. 1 below). In this case, a weak signal $\epsilon \cos \tilde{\omega} t$ generates a combination of harmonics $m\omega + k\tilde{\omega}$. The amplitudes of these harmonics increase with ϵ , and can reach a height of the order of the main

harmonic of the drive, even for very small ϵ . Thus, the weak signal can be amplified by a factor of up to several hundred.

- The amplification effects (Fig. 3) are not suppressed by a realistic amount of decoherence (dephasing and relaxation) in the system. Thus, e.g., currently available superconducting flux qubits with relatively short coherence times can be used as nanoscale, coherent amplifiers of weak signals in the frequency range of several hundred MHz.
- Noise (Fig. 4) of the order of the signal cannot suppress signal amplification (Fig. 5), which is also robust (but, of course, weaker) with respect to both: changing the frequency of the weak signal (Fig. 6a) and the parameters of the coupled-qubit system (Fig. 6a).

II. QUANTUM AMPLIFICATION WITH QUBITS

One of the challenging tasks for which superconducting qubits seem to be well suited is the amplification of a weak signal, a crucially important tool for both technological and scientific applications. For this goal, different types of linear or nonlinear resonance devices are commonly used (e.g., Ref. 16, 25). The problem of signal amplification becomes very difficult at the nano-scale. Here we demonstrate that two coupled qubits can be employed as a parametric amplifier [16] based on the effect of the parametric resonance between a weak signal and quantum oscillations between the quantum levels of the system, driven by an external ac signal (the pump signal). While the actual realization details of the qubits is irrelevant for the mathematics of the problem, we stress that the implementation of the proposed scheme is ideally suited for mesoscopic superconducting qubits because these are very controllable and versatile.

Two coupled qubits can be described by the Hamiltonian:

$$H = -\frac{1}{2} \sum_{j=1,2} [\Delta_j \sigma_z^j + \epsilon_j(t) \sigma_x^j] + g \sigma_x^1 \sigma_x^2 \quad (4)$$

where σ_z^j and σ_x^j are Pauli matrices corresponding to either the first ($j = 1$) or the second ($j = 2$) qubit; the eigenstates of σ_z^j are the basis states of the j th qubit at zero coupling.

To be more specific, let us consider two coupled nominally-identical superconducting persistent-current flux qubits (e.g., Ref. 13), where each of the latter consist of a superconducting loop interrupted by three Josephson junctions, along which persistent-currents can circulate controlled by applied magnetic fluxes. When two such loops are placed next to each other, so that they feel each other's magnetic fields, this situation naturally produces the "antiferromagnetic" coupling represented in Eq. (4) by the σ_x - σ_x term, with $g > 0$ (see, e.g., Ref. 26). More elaborate designs can produce a tunable coupling (see, e.g., Refs. 27, 28), with the amplitude and sign of g controlled externally by the magnetic flux, Φ_{coupl} , through the coupler loop [27] (see Fig. 1).

The state of each qubit is controlled by the magnetic flux $\Phi_e^{(j)} = f_e^{(j)}(t) \Phi_0$ through it, where $\Phi_0 = h/2e$ is the flux quantum. In the vicinity of $f_e^{(1)} = f_e^{(2)} = 1/2$, the ground state of each qubit is a symmetric superposition of states $|L\rangle$ and $|R\rangle$ with, respectively, clock- and counterclockwise circulating superconducting currents of the same magnitude I_p . In the basis $\{|L\rangle, |R\rangle\}^{(1)} \otimes \{|L\rangle, |R\rangle\}^{(2)}$ the two-qubit system can be described by the four-level Hamiltonian (4) with $\epsilon_j = I_p \Phi_0 \delta f_e^{(j)}$; here $\delta f_e^{(j)}(t)$ contains both the pump and the input signals. The tunnelling amplitudes Δ_j are usually fixed by the fabrication process, but can be tuned if one of the qubit junctions is replaced by two junctions in parallel, in a dc SQUID configuration (see, e.g., [29, 30]). The interaction constant g , as mentioned above, can be made tuneable using a coupler loop (Fig. 1). Note that the density matrix spectrum is directly related to the immediately measurable current/voltage spectrum in the tank, which was exploited in [31] to detect Rabi oscillations in a flux qubit.

For simplicity, we consider two identical qubits; that is, we assume $\Delta_1 = \Delta_2 = \Delta$. A direct diagonalization of the Hamiltonian (4) leads to the inter-level transition frequencies

$$\begin{aligned} \omega^{(1)} &= 2\sqrt{\Delta^2 + g^2}, & \omega^{(2)} &= \sqrt{\Delta^2 + g^2} - g, \\ \omega^{(3)} &= \sqrt{\Delta^2 + g^2} + g, & \omega^{(4)} &= 2g, \end{aligned} \quad (5)$$

which are tuneable by changing g . Therefore, $\omega^{(1)}, \dots, \omega^{(4)}$ can be adjusted to a desirable frequency, that was used below.

Let us drive the qubits simultaneously by a control ac pump signal, with frequency $\omega_{\text{pump}} = \omega$ and amplitude A , as well as a weak input signal with frequency $\omega_{\text{weak}} = \tilde{\omega}$ and amplitude $\epsilon \ll A$, to be amplified:

$$\epsilon_j(t) = A \sin(\omega t) + \epsilon \sin(\tilde{\omega} t) + \sqrt{2D} \xi_j(t) \quad (6)$$

where we also take into account a noise term (with intensity D) which can be due to fluctuations in the signals or an environmental noise. As an example, we consider white noise with zero mean: $\langle \xi(t) \rangle = 0$ and $\langle \xi_j(t) \xi_l(t') \rangle = \delta_{jl} \delta(t-t')$, where δ refers to either the Dirac delta function or the Kronecker delta. The qubit density matrix $\hat{\rho}$ can be written as

$$\hat{\rho} = \frac{1}{4} \sum_{a,b=0,x,y,z} \Pi_{ab} \sigma_a^1 \otimes \sigma_b^2. \quad (7)$$

This is a straightforward generalization of the standard representation of the single-qubit density matrix expression using the Bloch vector; the components Π_{ab} thus constitute what can be called the Bloch tensor. Then, the master equation,

$$\frac{d\hat{\rho}}{dt} = -i [\hat{H}(t), \hat{\rho}] + \hat{\Gamma} \hat{\rho}, \quad (8)$$

can be written down directly [see Eq. (12) in the Appendix], using the standard approximation for the dissipation operator $\hat{\Gamma}$ via the dephasing ($\Gamma_{\phi_1}, \Gamma_{\phi_2}$), and relaxation (Γ_1, Γ_2) rates, to characterize the intrinsic noise in the system. Also, for simplicity, hereafter we assume that the relaxation rates are the same for both identical qubits, i.e., $\Gamma_{\phi_1} = \Gamma_{\phi_2} = \Gamma_{\phi}$ and $\Gamma_1 = \Gamma_2 = \Gamma_r$, and the temperature is low enough, resulting in $Z_{T_2} = Z_{T_1} = 1$, where $Z_{T_j} = \tanh(\Delta_j/2k_B T_j)$ is the equilibrium value of the z -component of the Bloch vector.

In the limit of zero coupling, $g = 0$, there exists a solution of Eqs. (12) with no entanglement between the qubits. This solution can be written as a direct product of two independent density matrices expressed through their Bloch vectors:

$$\hat{\rho}_j = \frac{1}{2}(1 + X_j \sigma_x + Y_j \sigma_y + Z_j \sigma_z). \quad (9)$$

The components of the Bloch tensor Π_{ab} are all zero with the exception of

$$(\Pi_{ox}, \Pi_{oy}, \Pi_{oz}) = (X_1, Y_1, Z_1); \quad (\Pi_{xo}, \Pi_{yo}, \Pi_{zo}) = (X_2, Y_2, Z_2), \quad (10)$$

which are just the separate qubits' Bloch vector components. If the interaction is nonzero, $g \neq 0$, the entanglement between these qubits makes the components of the Bloch tensor nonzero, and such an entangled state can persist for some time even if the interaction is switched off later on.

III. SIMULATION RESULTS

Formally, the set of equations (12) might look complicated but these are just a set of fifteen coupled ordinary differential equations which can be easily integrated numerically [32]. Indeed, measuring time in units of $1/\Delta$, we numerically solved Eqs. (12) by the Euler method for two coupled qubits, driven by the field (6) with $\omega_{\text{pump}} = \omega = \omega^{(2)}$ and $\omega_{\text{weak}} = \tilde{\omega} = \omega^{(3)}$ [see Eq. (5)]. Our numerical integration produces a set of data for $\Pi_{a,b}(t)$ which can be analyzed using a Fourier transform. Thus, we can numerically evaluate the spectrum of $Z_1 = \Pi_{oz}$, defined as

$$S_Z(\omega) = \langle |Z_1(\omega)| \rangle, \quad (11)$$

and the similarly defined spectrum of $X_1 = \Pi_{ox}$. If one considers a flux qubit as a particular realization of our two-qubit parametric amplifier, then $Z_1(t)$ and $X_1(t)$ (and, thus, their spectra S_Z and S_X) can be directly obtained by using impedance measurements [33] of the circulating current in the first qubit of the proposed device. These spectra are shown in Fig. 2 for $g/\Delta = 1$. Below we will analyze the influence of a weak signal on S_Z and S_X .

When the weak signal is switched off [Fig. 2(a)], the spectrum of Z_1 exhibits several peaks corresponding to the harmonics, $\omega_m = m\omega$, of the applied drive ($A/\Delta = 15$). In contrast to the standard nonlinear response, where the spectrum starts from ω_1 and has harmonic peaks ω_m , whose heights *decrease* with m , in our two-qubit system, S_z starts with ω_2 and contains only even harmonics. The peak heights show a surprising *non-monotonic* dependence on m , with the two highest peaks occurring at $m = 20$ and $m = 22$. A somewhat similar non-monotonic peak dependence on the harmonic number is seen for S_X , the spectrum of the off-diagonal matrix element $X_1 = \Pi_{ox}$. Even though this spectrum starts with the main harmonic ω_1 , it contains only odd peaks which heights still show a non-monotonic dependence on m [Fig. 2(b)]. The super-indices in $\omega^{(1)}, \omega^{(1)}$, etc., refer to the level-splitting (intrinsic properties) of the qubits, while the lower indices in $\omega_1, \omega_2, \dots$ label the harmonics of the response to the input ac monochromatic drive. We measure all frequencies in units of the energy-splitting of independent qubits $\omega^{(2)}(g = 0)$, since this provides a characteristic frequency in the system which is fixed even if one tunes the inter-level frequencies $\omega^{(i)}(g)$.

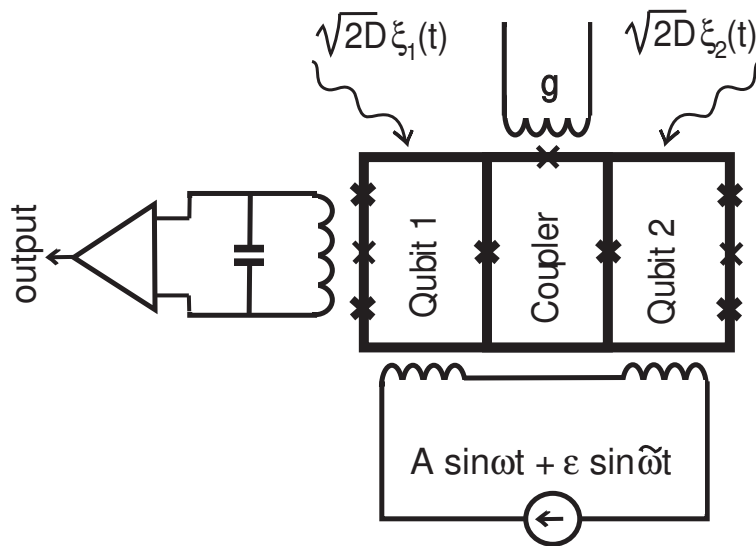


FIG. 1: Schematic diagram of two flux qubits (persistent current qubits) coupled via a coupler loop. Josephson junctions are represented by crosses, and their thickness indicate their Josephson critical currents (drawn not to scale). The qubit states and the amplitude and sign of the coupling constant g are controlled by the corresponding magnetic fluxes, $f_e^{(1,2)}$ and f_{coupler} (in units of Φ_0). Both the pumping drive and the weak signal $A \sin \omega t + \epsilon \sin \tilde{\omega} t$ are generated by a source in the bottom circuit. The left circuit is needed to pick up an output signal $Z_1(t)$. The top circuit controls the coupling g . Noise, shown by $\sqrt{2D}\xi_i(t)$, is coupled to each qubit.

All spectral peak heights are proportional to the drive amplitude A . Thus, a weak signal should produce a spectrum with strongly-suppressed peaks. This is consistent with our simulations for zero-drive amplitude $A = 0$ and weak-signal amplitude $\epsilon/\Delta = 0.1$. The resulting spectrum has only one peak, with an amplitude about 150 times lower than the highest peak of the S_Z spectrum for $A/\Delta = 15, \epsilon = 0$ [Fig. 2(a), the weak peak is shown there as “weak” and it is almost invisible].

When mixing the strong drive with a weak signal, the resulting spectrum S_Z at $A/\Delta = 15, \epsilon/\Delta = 0.1$ (i.e., $\epsilon/A = 1/150$) [Fig. 3(a)] strongly differs from the simple superposition of the two spectra described above, $S_Z(A/\Delta = 15, \epsilon = 0)$ and $S_Z(A = 0, \epsilon/\Delta = 0.1)$. It is remarkable that *the weak signal produces a considerable change in the spectrum*: it generates peaks at combination frequencies, $k\omega + l\tilde{\omega}$, with integer k and l ; their heights are determined by the weak signal but can be of the order of the highest peak in $S_Z(A/\Delta = 15, \epsilon = 0)$. Interestingly, the enhancement of combination-frequency harmonics occurs by borrowing some energy from the pumping drive, which own harmonics (harmonics existing at $\epsilon = 0$) decay when the weak signal is applied. Indeed, if one compares the spectrum at $\epsilon = 0$ shown by red dotted lines, with the spectrum at $\epsilon/\Delta = 0.1$ shown by black solid lines in Fig. 3a, one can see that the heights of the harmonics at $\epsilon = 0$ are higher than the corresponding peaks at $\epsilon/\Delta = 0.1$, even though the total energy pumped in the system is larger when both the pumping drive and the weak signal are applied.

The heights of the combination-frequency peaks increase with the weak signal amplitude, ϵ , followed by saturation at large values of ϵ . Of course, the heights of the combination-frequency peaks tend to zero when $\epsilon \rightarrow 0$. It is clearly seen [Fig. 3(b)] that their height can be approximated by a linear function, $\beta\epsilon$, for the weak signal amplitude in the range $0 < \epsilon/A < 0.005$, with an *amplification coefficient* β of about 100. This level of amplification is remarkable.

It is also useful to stress that many peaks associated with different combinations of two frequencies, $k\omega_{\text{pump}} + l\omega_{\text{weak}}$, appear in the spectrum of S_Z for different integers k and l . In other words, the spectrum has many combination-frequency harmonics with different intensities. This allows to pick up the signal on a frequency which better fits the frequency of a weak signal to a desirable frequency range. Note that it is usually hard to predict which peak should be the highest one [see Fig. 3 with highest peak marked as $I(\epsilon)$]. However, by measuring the output signal I_{\pm} of the first mixing harmonics, $\omega_{\text{weak}} \pm \omega_{\text{pump}}$, usually allows to pick up a strongly amplified signal. For instance, the ratio of the highest peak I_e to I_{\pm} is about 1.7 in our simulations shown in Fig. 3a. Therefore, choosing the harmonics $\omega_{\text{weak}} \pm \omega_{\text{pump}}$ would be a good guide to observe the predicted signal amplification.

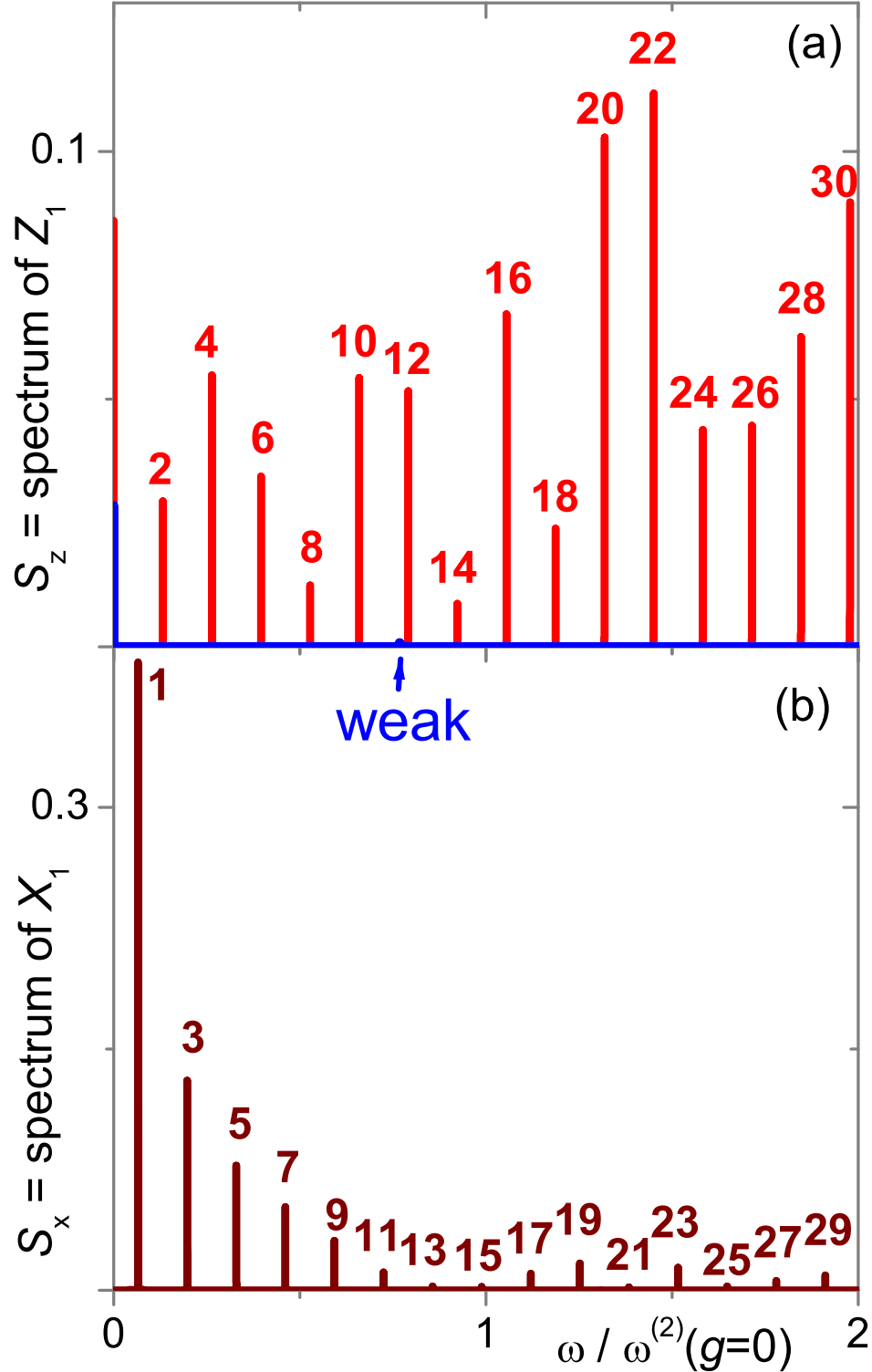


FIG. 2: (Color online) The spectrum S_Z of the Z_1 matrix element (responsible for the occupation of the excited level of the first qubit) is shown for dephasing and relaxation given by $\Gamma_\phi/\Delta = \Gamma_r/\Delta = 10^{-3}$ (we use the same Γ_ϕ and Γ_r for all results reported in this article). (a) When the weak signal amplitude is equal to zero ($\epsilon = 0$) and when the reduced-drive amplitude $A/\Delta = 15$, the ac monochromatic drive fed into the two-qubit amplifier is converted into a set of even harmonics $\omega_m = m\omega$, with $m = 2, 4, 6, \dots$. Note the absence of response at $\omega_1 = \omega$ (no peak there). For comparison, S_Z is shown in blue and indicated by the blue arrow for zero-drive amplitude $A = 0$ and weak signal $\epsilon/\Delta = 0.1$. Only one very small peak is hardly seen, indicated by the blue arrow, corresponding to $2\omega_{\text{weak}}$. (b) Spectrum S_X of the off-diagonal matrix element X_1 (zero signal case). The same ac monochromatic drive fed into the amplifier is converted into a set of odd harmonics for S_X : $m = 1, 3, 5, \dots$. Note that (a) and (b) show very unusual non-monotonic spectra. The observed non-monotonicity in the system response can be seen as a fingerprint of the qubits, characterizing their dynamical nonlinear response.

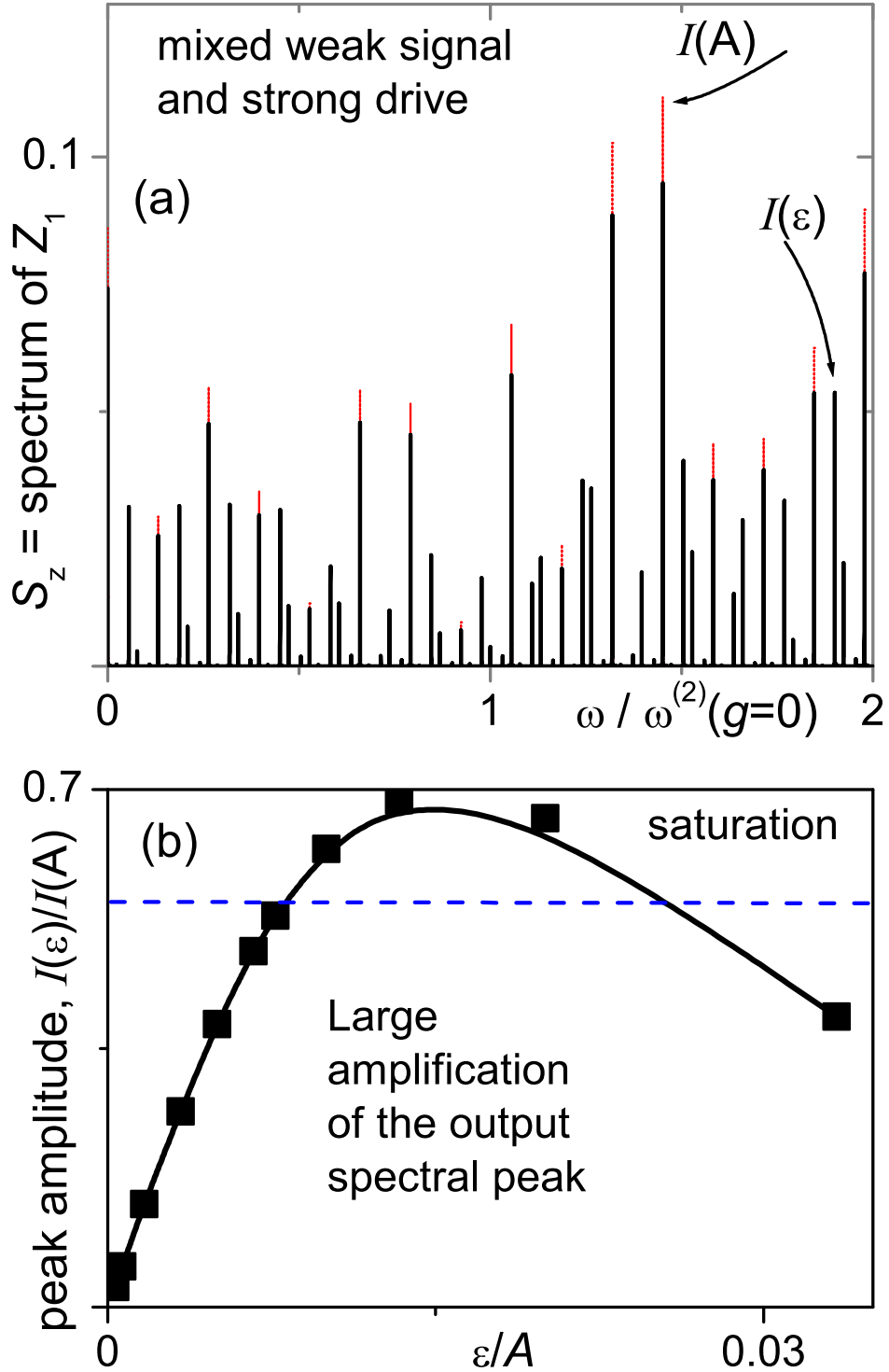


FIG. 3: (Color online) (a) The amplification of a weak signal $\epsilon/\Delta = 0.1$ by a strong drive $A/\Delta = 15$ (i.e., $\epsilon/A = 1/150$) can be seen in the spectrum of S_z shown by the black solid lines. The spectrum obtained is *not a simple superposition* of the two spectra $S_z(A/\Delta = 15, \epsilon = 0)$ (also shown here by red vertical dotted peaks) and $S_z(A = 0, \epsilon/\Delta = 0.1)$ [see also red and blue peaks in Fig. 2(a)]. Instead, a combination of harmonics appears for $k\omega + l\tilde{\omega}$, with integer k and l . The height of these peaks is almost proportional to $\beta\epsilon$, for $0 < \epsilon/A < 0.005$, and it is strongly enhanced by a factor $\beta \sim 100$. The enhanced peak is marked by an arrow with symbol $I(\epsilon)$. Note that this peak is absent in Fig. 2(a). (b) Normalized output amplitude $I(\epsilon)/I(A)$ (ratio of the heights of the highest mixed peak $I(\epsilon)$ to the highest peak $I(A)$ of the spectrum at $\epsilon = 0$) as a function of the reduced weak signal amplitude ϵ/A . This dependence shows an almost-linear increase of the peak height with ϵ for small ϵ/A , followed by saturation and even decay at relatively large ϵ/A .

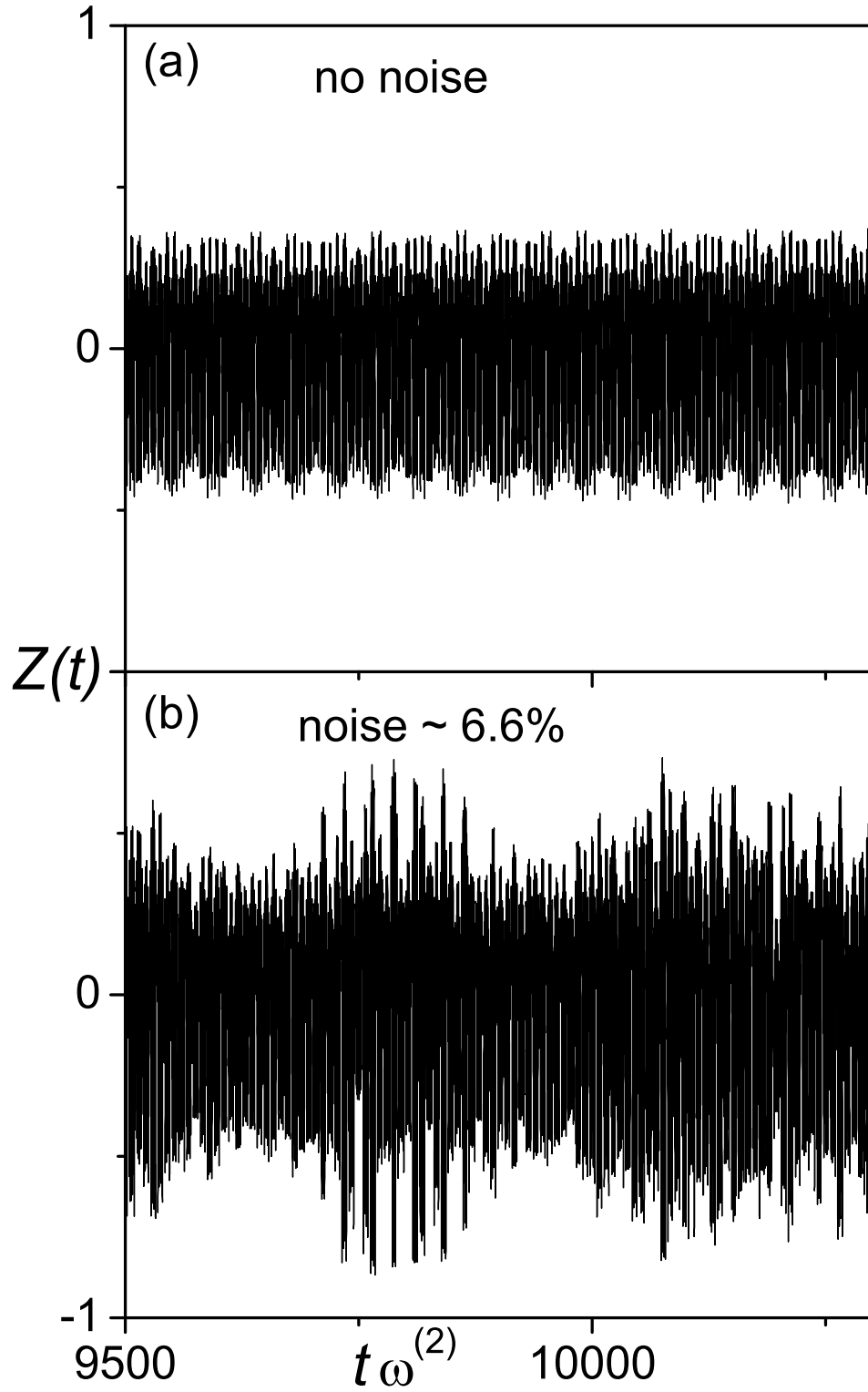


FIG. 4: (Color online) Trajectories $Z_1(t)$ for different noise levels: $\sqrt{D}/\epsilon = 0$ for (a) and $\sqrt{D}/\epsilon = 0.066$ for (b). All other parameters are the same as in Fig. 3a. As seen from (b), the applied white noise considerably affects the time dependence of $Z_1(t)$, making trajectories quite noisy with respect to the noiseless situation shown in (a).

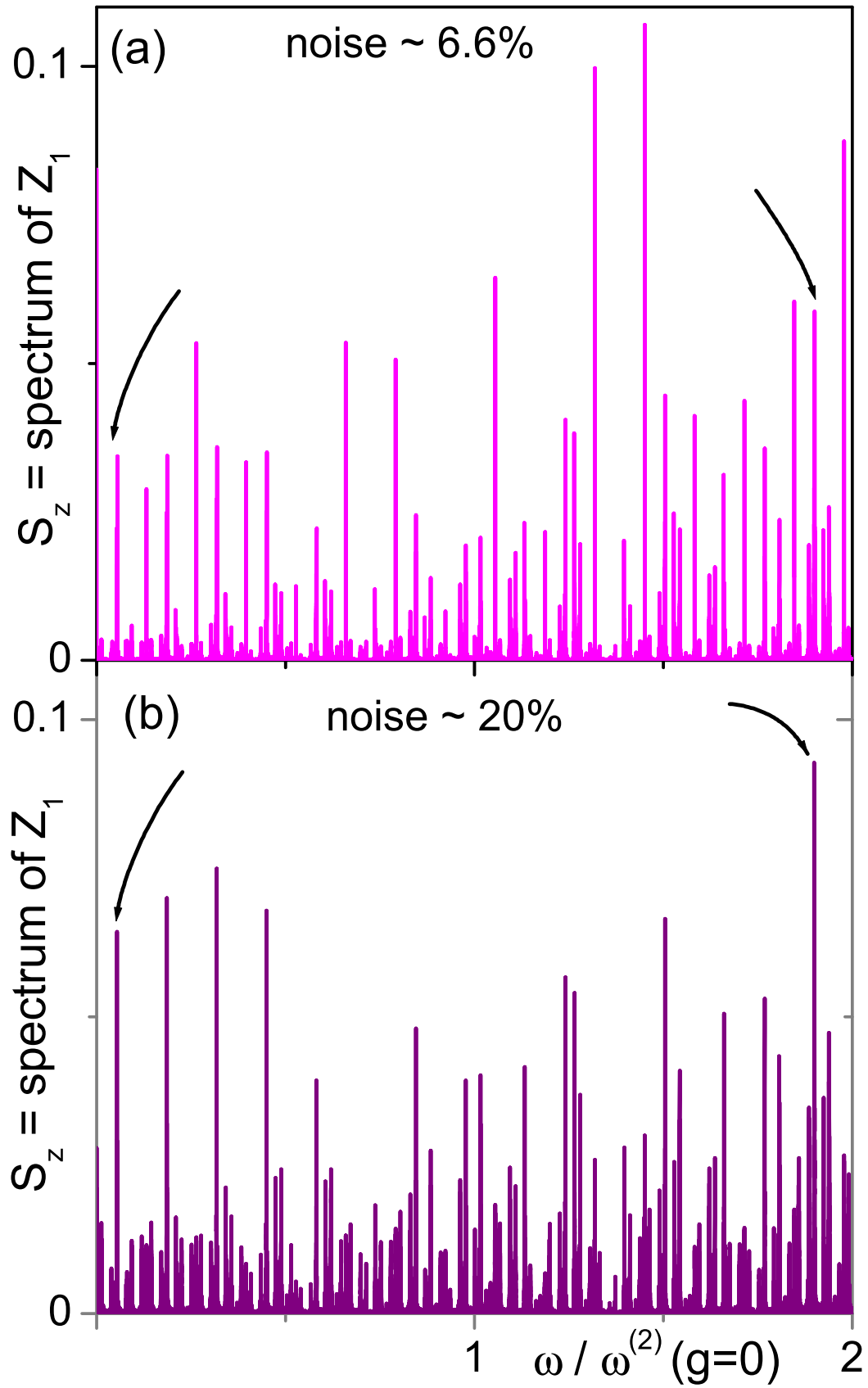


FIG. 5: (Color online) Spectrum $S_z(\omega)$ for the same parameters used in Fig. 3 and different noise levels $\sqrt{D}/\epsilon = 0.066$ for (a) and 0.2 for (b). One can clearly see the mixed (pump-signal) peaks for several combination-frequencies $k\omega_{\text{pump}} + l\omega_{\text{weak}}$, even at high noise levels, when the trajectories $Z_1(t)$ shown in Fig. 4 are very noisy.

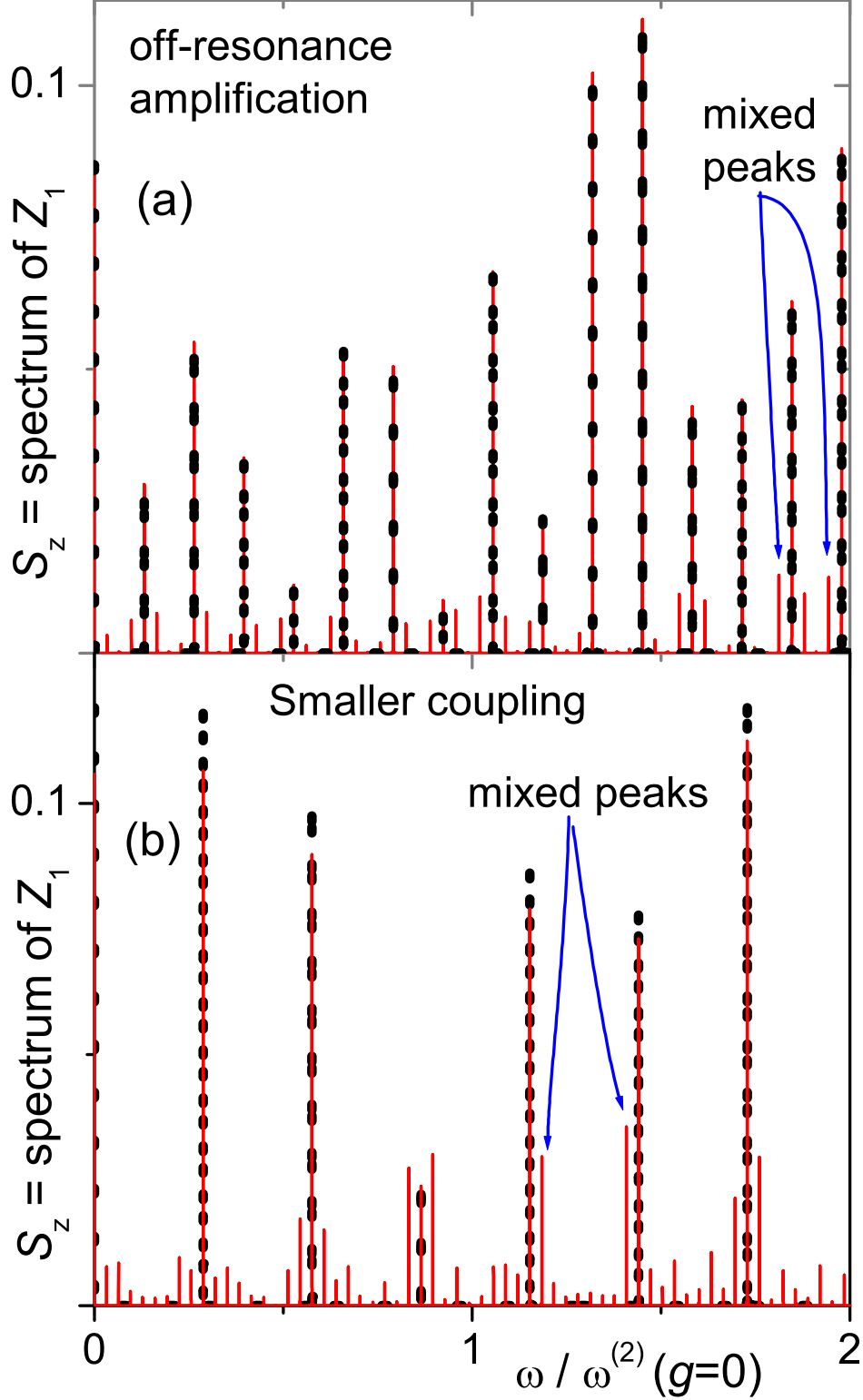


FIG. 6: (Color online) Amplification of a weak signal away from the optimal regime. (a) Spectrum S_z for off-resonance frequency $\omega_{\text{weak}} = 1.113\omega^{(3)}(g = 1)$ of a weak signal shown by red thin solid line. All other parameters of the simulations are the same as in Fig. 3. The thick black dotted line corresponds to the simulations with zero signal, thus, highlighting the combination-frequency amplified harmonics as red lines with no black dots on top. One can see that the amplification of off-resonance signal is weaker, but still remarkable with amplification factor β about 30. (b) Spectrum of S_z for weakly coupled qubits $g/\Delta = 0.1$ and weak signal amplitude $\epsilon/A = 24$, as shown by the red thin solid line; all other parameters are as in Fig. 3 and $A/\Delta = 12$. The same simulations but with zero signal is shown by a thick black dotted line to highlight the amplified mixed peaks. The estimated amplification factor β is about 10.

IV. NOISE INFLUENCE

Since a weak signal can be considerably amplified by a strong drive in our parametric amplifier, one can wonder if an uncontrollable noise could also be amplified making the weak signal indistinguishable. To check this we performed simulations at different noise levels choosing all other parameters as in Fig. 3, i.e., $A/\Delta = 15$, and $\epsilon/A = 1/150$. A noise with intensity of the order of 6.6% with respect to the weak signal (i.e., $\sqrt{D}/\epsilon \sim 0.066$) has already considerably affected the time dependence of the measured signal (see, Fig. 4), but it does not strongly influence the spectrum of $S_Z(\omega)$, as seen in Fig. 5a. The reason for this is that the noise contains all frequencies (or at least a broad frequency spectrum), thus, its energy pumped in the signal harmonic is relatively small.

Even stronger noise, $\sqrt{D}/\epsilon = 0.2$, is still not enough to suppress the peaks attributed to the weak signal. Moreover, a sort of stochastic resonance (increase of the peak heights with noise) [34] is also seen on Fig. 5b. Therefore, the proposed two-qubit parametric amplifier is robust with respect to noise and, moreover, the noise can even be used to further amplify the signal.

V. AWAY FROM THE OPTIMAL REGIME: ROBUST AMPLIFICATION OF TWO-QUBIT AMPLIFIER

In order to realize the strongest amplification of a weak signal (optimal working regime), a tuneable coupling must be used. In other words, the coupling should be tuned to adjust a level splitting frequency $\omega^{(i)}$ to the frequency ω_{weak} of the applied weak signal. This adjustment cannot be always realized. Thus, the amplification of a weak signal of an arbitrary frequency (different from the level splitting) is worth studying. As we expected, the amplification of the weak signal on the frequency $\omega_{\text{weak}} = 1.113\omega^{(3)} \neq \omega^{(i)}$ is weaker (Fig. 5a) by a factor of about 3.5 (ratio of the highest combination-frequency peaks in Figs. 3 and 6) with respect to the optimal amplification $\omega_{\text{weak}} = \omega^{(3)}$, i.e., in the case when the signal frequency is equal to the level splitting. Nevertheless, this amplification is still strong enough (β is about 20–30) allowing to use the proposed amplifier for a weak signal with arbitrary frequency.

A similar situation occurs if the qubit coupling is not strong enough to reach the optimal regime (see Fig. 6b). Indeed, the amplification of a weak signal ($\epsilon/\Delta = 0.5$) by the strong drive ($A/\Delta = 12$) is weaker, but still essential (β about 10) for the coupling $g = 0.1$.

VI. CONCLUSIONS

The spectrum of two coupled qubits driven by an ac signal with the frequency in resonance with inter-level transitions has an unusual structure, with a hierarchy of harmonic peaks with heights non-monotonically dependent on the harmonic's number. This peak-height hierarchy is a fingerprint of any two-qubit system and can be used to characterize both individual qubit parameters as well as the interqubit coupling.

Exploiting the analogy between a parametric amplifier and a system of two coupled qubits, we propose a method of amplification of a weak signal via its mixing with a strong pump signal applied to the two-qubit system. If both signals are relatively close to the inter-level transitions in the four-level quantum system (which can be achieved by tuning the qubit coupling), then the amplification coefficient can be of the order of 100. When the weak signal frequency is different from the inter-level splitting then the amplification is still strong enough, allowing the proposed amplifier to work efficiently both in inter-level resonance and off inter-level resonance regimes. Weakening the qubit coupling also suppresses a weaker signal enhancement, thus, requiring strongly-coupled qubits for this remarkable parametric amplification.

We also show that noise, which is of the order of a weak signal, can strongly affect the time dependence of the output signal $Z_1(t)$, but it modifies much weakly the spectrum S_Z . Therefore, the proposed amplifier can work efficiently in noisy conditions. This large amplification offers a different way of using multiqubit circuits as parametric amplifiers.

VII. ACKNOWLEDGMENTS

We acknowledge partial support from FRSF (Grant No. F28.21019) and EPSRC (No. EP/D072518/1). FN acknowledges partial support from the National Security Agency, Laboratory of Physical Science, Army Research Office, National Science Foundation grant No. 0726909, DARPA, AFOSR, JSPS-RFBR contract No.09-02-92114, MEXT Kakenhi on Quantum Cybernetics, and the JSPS-FIRST Program.

VIII. APPENDIX: MASTER EQUATIONS FOR THE DENSITY MATRIX COMPONENTS

The master equation (7) can be explicitly written as follows [34]:

$$\begin{aligned}
\dot{\Pi}_{0x} &= \Delta_2 \Pi_{0y} - \Gamma_{\phi 2} \Pi_{0x} \\
\dot{\Pi}_{0y} &= -\Delta_2 \Pi_{0x} + \epsilon_2(t) \Pi_{0z} - 2g \Pi_{xz} - \Gamma_{\phi 2} \Pi_{0y} \\
\dot{\Pi}_{0z} &= -\epsilon_2(t) \Pi_{0y} + 2g \Pi_{xy} - \Gamma_2 (\Pi_{0z} - Z_{T2}) \\
\\
\dot{\Pi}_{x0} &= \Delta_1 \Pi_{y0} - \Gamma_{\phi 1} \Pi_{x0} \\
\dot{\Pi}_{y0} &= -\Delta_1 \Pi_{x0} + \epsilon_1(t) \Pi_{z0} - 2g \Pi_{zx} - \Gamma_{\phi 1} \Pi_{y0} \\
\dot{\Pi}_{z0} &= -\epsilon_1(t) \Pi_{y0} + 2g \Pi_{yx} - \Gamma_1 (\Pi_{z0} - Z_{T1}) \\
\\
\dot{\Pi}_{xx} &= \Delta_2 \Pi_{xy} + \Delta_1 \Pi_{yx} - (\Gamma_{\phi 1} + \Gamma_{\phi 2}) \Pi_{xx} \\
\dot{\Pi}_{xy} &= -2g \Pi_{0z} - \Delta_2 \Pi_{xx} + \Delta_1 \Pi_{yy} + \epsilon_2(t) \Pi_{xz} - (\Gamma_{\phi 1} + \Gamma_{\phi 2}) \Pi_{xy} \\
\dot{\Pi}_{yx} &= -2g \Pi_{z0} - \Delta_1 \Pi_{xx} + \Delta_2 \Pi_{yy} + \epsilon_1(t) \Pi_{xz} - (\Gamma_{\phi 1} + \Gamma_{\phi 2}) \Pi_{yx} \\
\dot{\Pi}_{xz} &= 2g \Pi_{0y} - \epsilon_2(t) \Pi_{xy} + \Delta_1 \Pi_{yz} - (\Gamma_{\phi 1} + \Gamma_2) \Pi_{xz} \\
\dot{\Pi}_{zx} &= 2g \Pi_{y0} - \epsilon_1(t) \Pi_{yx} + \Delta_2 \Pi_{zy} - (\Gamma_{\phi 2} + \Gamma_1) \Pi_{zx} \\
\dot{\Pi}_{yy} &= -\Delta_1 \Pi_{xy} - \Delta_2 \Pi_{yx} + \epsilon_2(t) \Pi_{yz} + \epsilon_1(t) \Pi_{zy} - (\Gamma_{\phi 1} + \Gamma_{\phi 2}) \Pi_{yy} \\
\dot{\Pi}_{yz} &= -\Delta_1 \Pi_{xz} - \epsilon_2(t) \Pi_{yy} + \epsilon_1(t) \Pi_{zz} - (\Gamma_{\phi 1} + \Gamma_2) \Pi_{yz} \\
\dot{\Pi}_{zy} &= -\Delta_2 \Pi_{zx} - \epsilon_1(t) \Pi_{yy} + \epsilon_2(t) \Pi_{zz} - (\Gamma_1 + \Gamma_{\phi 2}) \Pi_{zy} \\
\dot{\Pi}_{zz} &= -\epsilon_1(t) \Pi_{yz} - \epsilon_2(t) \Pi_{zy} - (\Gamma_1 + \Gamma_2) (\Pi_{zz} - Z_{T1} Z_{T2})
\end{aligned} \tag{12}$$

where the symbols are explained in Eqs. (4-10). In the absence of qubit-qubit coupling, $g = 0$, the first three equations in (12) describe the evolution of the Bloch vector components $(\Pi_{0x}, \Pi_{0y}, \Pi_{0z})$ of qubit 1, and the second three equations in (12) describe those $(\Pi_{x0}, \Pi_{y0}, \Pi_{z0})$ of qubit 2.

-
- [1] M. Le Bellac, *A Short Introduction to Quantum Information and Quantum Computation* (Cambridge University Press, 2006).
- [2] J.Q. You, F. Nori, *Nature* **474**, 589 (2011).
- [3] J.Q. You and F. Nori, *Physics Today* **58**, No. 11, 42 (2005).
- [4] I. Buluta, F. Nori, *Science* **326**, 108 (2009).
- [5] I. Buluta, S. Ashhab, F. Nori, *Reports on Progress in Physics*, in press (2011), arXiv:1002.1871.
- [6] A.Yu. Smirnov, S. Savel'ev, L.G. Mourokh, F. Nori, *Euro. Phys. Lett.* **80**, 67008 (2007).
- [7] A.M. Zagoskin, S. Savel'ev, F. Nori, *Phys. Rev. Lett.* **98**, 120503 (2007).
- [8] A.L. Rakhmanov, A.M. Zagoskin, S. Savel'ev, and F. Nori, *Phys. Rev. B* **77**, 144507 (2008).
- [9] O. Astafiev, A. M. Zagoskin, A. A. Abdumalikov, Jr., Y. A. Pashkin, T. Yamamoto, K. Inomata, Y. Nakamura, and J. S. Tsai, *Science* **327**, 840 (2010); A. A. Abdumalikov, O. Astafiev, A. M. Zagoskin, Yu. A. Pashkin, Y. Nakamura, J. S. Tsai, *Phys. Rev. Lett.* **104**, 193601 (2010).
- [10] S. M. Girvin, M. H. Devoret and R. J. Schoelkopf, *Phys. Scr.* **T137**, 014012 (2009).
- [11] G. Wendin and V. S. Shumeiko, in: M. Rieth and W. Schommers (eds.), *Handbook of Theoretical and Computational Nanotechnology*, v. 3 (American Scientific Publishers, 2006); also: arXiv:cond-mat/0508729.
- [12] A. Zagoskin and A. Blais, *Physics in Canada* **63**, 215 (2007); also: arXiv:0805.0164.
- [13] J.E. Mooij, T.P. Orlando, L. Levitov, L. Tian, C.H. van der Wal, and S. Lloyd, *Science* **285**, 1036 (1999).
- [14] T.P. Orlando, J.E. Mooij, L. Tian, C.H. van der Wal, L. Levitov, S. Lloyd, J.J. Mazo, *Phys. Rev. B* **60**, 15398 (1999).
- [15] A.M. Zagoskin, *Quantum Engineering*, Cambridge University Press (2011).
- [16] V. Damgov, *Nonlinear and Parametric Phenomena: Theory and Applications in Radiophysical and Mechanical Systems* (World Scientific, Singapore, 2001).
- [17] J.H. Posthumus, *Reports on Progress in Physics* **67**, 623 (2004).
- [18] C. Ciuti, P. Schwendemann, A. Quattropani, *Semicond. Sci. Tech.* **18**, S279 (2003).
- [19] M. Muck, R. McDermott, *Supercond. Sci. Tech.* **23**, 093001 (2010).
- [20] R. Vijay, M.H. Devoret, I. Siddiqi, *Rev. Sci. Inst.* **80**, 111101 (2009).
- [21] J. R. Johansson, G. Johansson, C. M. Wilson, F. Nori, *Phys. Rev. Lett.* **103**, 147003 (2009); *Phys. Rev. A* **82**, 052509 (2010).
- [22] P. D. Nation, J. R. Johansson, M. P. Blencowe, F. Nori, arXiv:1103.0835.
- [23] A.D. Boardman, V.V. Grimalsky, Y.S. Kivshar, S.V. Koshevaya, M. Lapine, N.M. Litchinitser, V.N. Malnev, M. Noginov, Y.G. Rapoport, V.M. Shalaev, A.B. Kozyrev, D.W. van der Weide, *J. Phys. D - Applied Physics* **41**, 173001 (2008).
- [24] A.A. Clerk, M.H. Devoret, S.M. Girvin, F. Marquardt, R.J. Schoelkopf, *Rev. Mod. Phys.* **82** 1155 (2010).

- [25] S. Savel'ev, A.L. Rakhmanov, and F. Nori, Phys. Rev. E **72**, 056136 (2005); New J. Phys. **7**, 82 (2005).
- [26] M. Grajcar, A. Izmailkov, S.H.W. van der Ploeg, S. Linzen, E. Il'ichev, Th. Wagner, U. Hubner, H.-G. Meyer, Alec Maassen van den Brink, S. Uchaikin, and A.M. Zagoskin, Phys. Rev. B **72**, 020503(R) (2005).
- [27] S.H.W. van der Ploeg, A. Izmailkov, A. Maassen van den Brink, U. Huebner, M. Grajcar, E. Il'ichev, H.-G. Meyer, and A.M. Zagoskin, Phys. Rev. Lett. **98**, 057004 (2007).
- [28] M. Grajcar, Y.X. Liu, F. Nori, A.M. Zagoskin, Phys. Rev. B **74**, 172505 (2006); S. Ashhab, S. Matsuo, N. Hatakenaka, F. Nori, Phys. Rev. B **74**, 184504 (2006); S. Ashhab, A.O. Niskanen, K. Harrabi, Y. Nakamura, T. Picot, P.C. de Groot, C.J.P.M. Harmans, J.E. Mooij, F. Nori, Phys. Rev. B **77**, 014510 (2008).
- [29] J.Q. You, Y.X. Liu, C.P. Sun, F. Nori, Phys. Rev. B **75**, 104516 (2007).
- [30] F.G. Paauw, A. Fedorov, C.J.P.M. Harmans, and J.E. Mooij, Phys. Rev. Lett. **102**, 090501 (2009).
- [31] E. Il'ichev, N. Oukhanski, A. Izmailkov, T. Wagner, M. Grajcar, H.-G. Meyer, A. Smirnov, A. Maassen van den Brink, M.H.S. Amin, and A.M. Zagoskin, Phys. Rev. Lett. **91**, 097906 (2003).
- [32] P. Moin, *Fundamentals of Engineering Numerical Analysis* (Cambridge University Press; 2010).
- [33] E. Il'ichev, N. Oukhanski, T. Wagner, H.-G. Meyer, A. Yu. Smirnov, M. Grajcar, A. Izmailkov, D. Born, W. Krech, and A. Zagoskin, Low Temp. Phys. **30**, 620 (2004).
- [34] A.N. Omelyanchouk, S. Savel'ev, A.M. Zagoskin, E. Il'ichev, F. Nori, Phys. Rev. B **80**, 212503 (2009); S. Savel'ev, A.M. Zagoskin, A.N. Omelyanchouk, F. Nori, Chem. Phys. **375** 180 (2010).